Operando Spectro-electrochemical investigations of Pt and Pt-alloys as fuel cell catalysts

Nagra, H.J.

Chapter 2

A laboratory-based electrochemical NAP-XPS system for operando electrocatalysis studies

Abstract

During electrocatalytic reactions, the electrode, adsorbates, electrolyte ions, and solvent molecules at the electrode-electrolyte interface each play an important role. Electrochemical X-ray photoelectron spectroscopy (XPS) holds great promise for deciphering these roles, providing the oxidation state or bonding environment of every element present at the interface. However, combining the vacuum required for XPS with the wet environment needed for electrochemistry constitutes a technical challenge, requiring purpose-built instrumentation and spectro-electrochemical cell design. Here, we present a laboratory-based electrochemical XPS instrument optimized for *operando* studies on nano-structured electrocatalysts. We show that using a spectro-electrochemical cell design based on a membrane-catalyst-graphene assembly, the system is able to probe the electrode surface, interfacial water, and interfacial ions under well-defined potential control. Importantly, the system facilitates the transport of any molecule or ion towards the working electrode, facilitating measurements under a wide variety of electrocatalytic conditions. This is exemplified for the oxygen reduction reaction.

This Chapter has been published in Vacuum:

Javed, H.; Kolmeijer, K.; Klein, N.; Trindell, J. A.; Schneider, G.; Mom, R. V. A Laboratory-Based Electrochemical NAP-XPS System for Operando Electrocatalysis Studies. *Vacuum* 2025, *231* (PA), 113755. https://doi.org/10.1016/j.vacuum.2024.113755.

Chapter 2 : A laboratory-based electrochemical NAP-XPS system for *operando* electrocatalysis studies

2.1 Introduction

An atomic-level understanding of the relationship between the applied potential and the electrode-electrolyte interface structure is crucial for advancing electrochemical systems, including batteries, electrolyzers, and fuel cells[1–4]. X-ray photoelectron spectroscopy (XPS) is among the most powerful characterization techniques for achieving this understanding[5–14], offering insights into oxidation states, bonding environments, and the local electrostatic potential[15](in e.g. the double layer). However, the vacuum required for XPS measurements makes in situ measurements under electrochemical conditions non-trivial. To interface the wet environment needed for electrochemistry with the vacuum required for XPS, several experimental arrangements have been developed, such as the dip-and-pull method[16–18], polymer electrolyte membrane approach[19,20] and graphene window-based approaches[21–23]. This has made it possible to study several important electrochemical systems, such as the oxygen evolution reaction[24–26] and the CO_2 reduction reaction[27,28].

While these applications highlight the potential of electrochemical XPS, the current reliance on synchrotron facilities limits access to the technique. Wider use could be achieved through the development of laboratory-based electrochemical XPS. First efforts in this direction have emerged[29–33], making use of the lab-based near-ambient-pressure XPS (NAP-XPS) instrumentation that has recently become available. For example, Liu et al. employed a Cr source to perform dip-and-pull type measurements using tender X-rays[29], in direct analogy to the dip-and-pull set-ups available at synchrotrons. A different approach was used by Haug et al.[33], who used an Al soft X-ray source in combination with a tilted thin film cell. Both approaches rely on the formation of a 10-30 nm electrolyte film on the electrode, which is thick enough for a realistic electrode-electrolyte interface structure to form, but thin enough for photoelectrons to traverse in order to reach the electron analyzer. Due to the limited mass transport through the ultrathin electrolyte film, this strategy is primarily suited for the study of the electrode-electrolyte interface under non-faradaic conditions, i.e. when little electrochemical current passes[20].

To extend the applicability of laboratory electrochemical XPS to electrocatalytic systems with significant electrochemical current, we present a system based on a membrane-electrode-assembly type cell, analogous to fuel cells and electrolyzers. This approach builds on the membrane cells developed in the Gericke group at the BESSY II synchrotron, which have proven successful for the study of e.g. oxygen evolution electrocatalysis[21,34–39] at significant current density. Here, we introduce the use of a porous polycarbonate membrane in the MEA, which facilitates the transport of any molecular or ionic reactant to the working electrode, enabling in situ studies on a wide variety of electrocatalytic reactions. We demonstrate the capabilities of the instrument using the oxidation of Pt, adsorption of SO_4^{2-}, and the oxygen reduction reaction.

2.2 System design

The electrochemical XPS setup exhibits a modular arrangement (as shown in Figure 2.1), consisting of 1) a load-lock with a manipulator that holds the electrochemical cell, 2) the main chamber, to which the 3) X-ray source, 4) ultra-high-vacuum (UHV) pumping section and 5) the electron analyzer are attached. In addition, electrolyte/gas supply and safety interlock systems support the operation of the set-up. Most components in the system are standard commercial components. However, the load lock, main chamber, and the support systems have been designed in-house specifically for electrochemical experiments. In the coming sections, we will focus on the design of the most crucial part of the set-up, the cell design. A detailed description of other components of the system is provided in the supporting information (supplementary information A2.1-2.6).

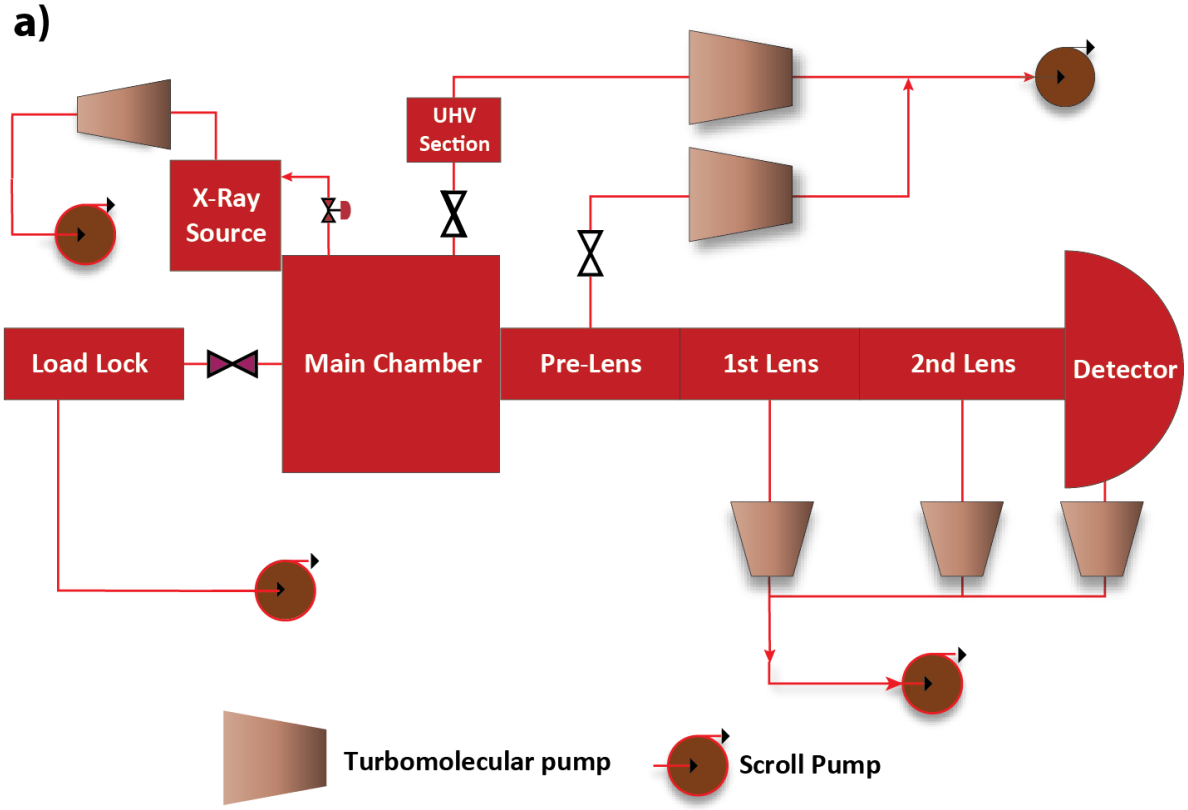

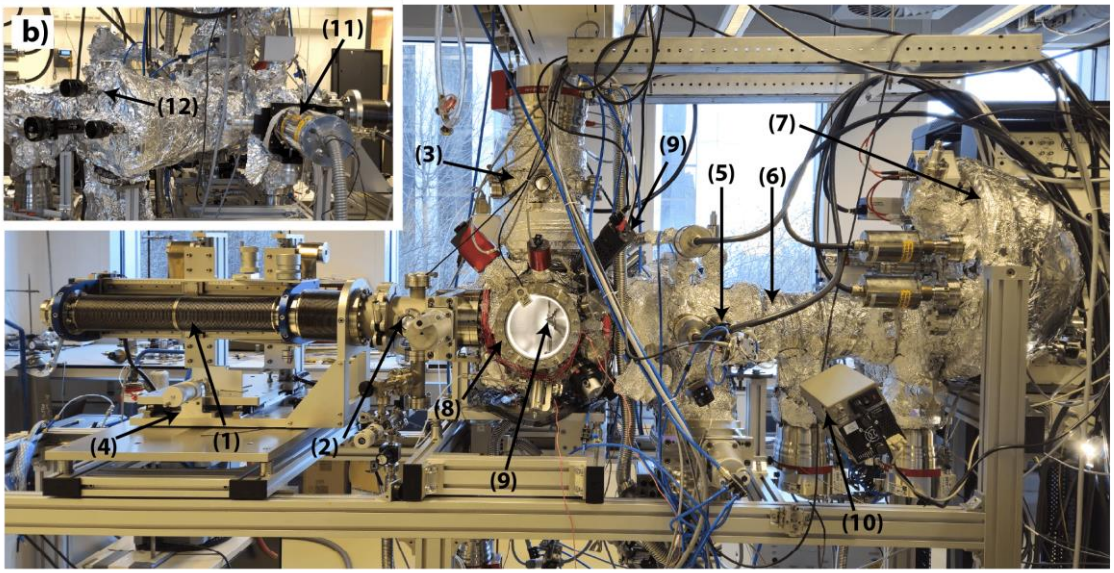

Figure 2.1 : Overview of the EC-NAP-XPS. a) Schematic diagram showing the layout of the system and b) Labelled system photograph displaying a detailed view of the NAP-XPS setup

i) In situ spectro-electrochemical (EC-XPS) cell extension

The electrochemical extension contains the electrochemical cell, electrolyte and electrical connections, and safety valves (Figure 2.2 and Figure 2.3). The extension contains a fixed and an interchangeable part. The fixed part is inserted into the tube of the manipulator (see supplementary information A2.1), separating it from the vacuum and contains the electrolyte lines along with the electrical connections that remain mounted on the inner manipulator tube. The interchangeable part comprises of the electrochemical cell that can be removed from the manipulator, facilitating easy sample/cell exchange.

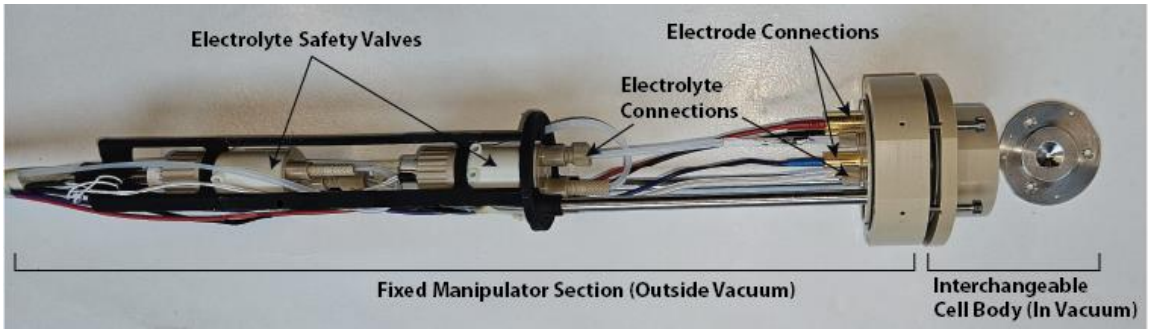

Figure 2.2 : Electrochemical manipulator construction

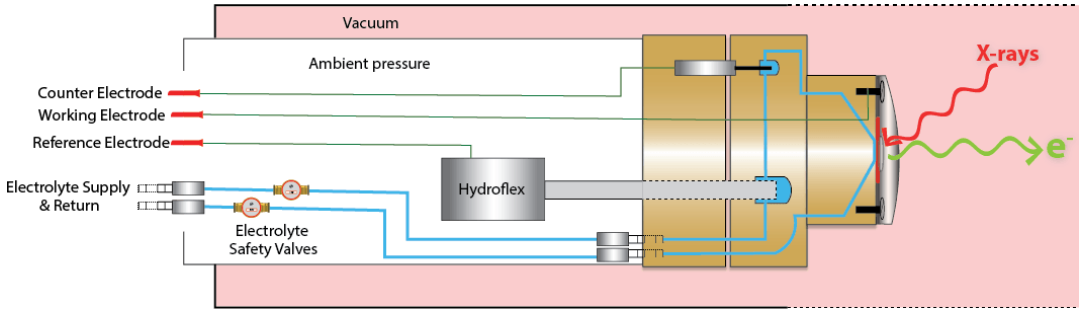

Figure 2.3 : Schematic diagram of the electrochemical manipulator

Figure 2.4 (A, B and C) show the detailed component view of the exchangeable part, i.e. the electrochemical cell. In Figure 2.4 A, the cell body (1) is made from PEEK using 3D printing (Bond3D Production BV), with channels for electrolyte flow (2) as well as connections for reference and counter electrodes built into the cell body.

The reference electrode (3) is a standard hydroflex (Gaskatel) which is screwed in via a brass coupling into a dedicated cavity in the cell body. The design choice of having the reference electrode horizontally at the back of the cell outside the vacuum (Figure 2.3) allows us to use the larger version of the hydroflex, which is more stable over the long run. The counter electrode (4) is a platinum rod attached to the cell body by a PEEK coupling and extends into the electrolyte channel. This Pt rod can be disassembled from its coupling to be cleaned and annealed separately. Figure 2.4 B shows the top view of the cell; a membrane electrode assembly (working electrode) is mounted underneath the titanium contact plate (6) which is in contact with a brass coupling (5) screwed through the PEEK body of the cell, establishing an electrical connection to the working electrode. The top plate contains a 2 mm opening, which is the measurement area for XPS (7). Electrical connection between the cell's electrodes and the fixed manipulator section is established via spring contacts, minimizing the amount of screws involved in cell mounting.

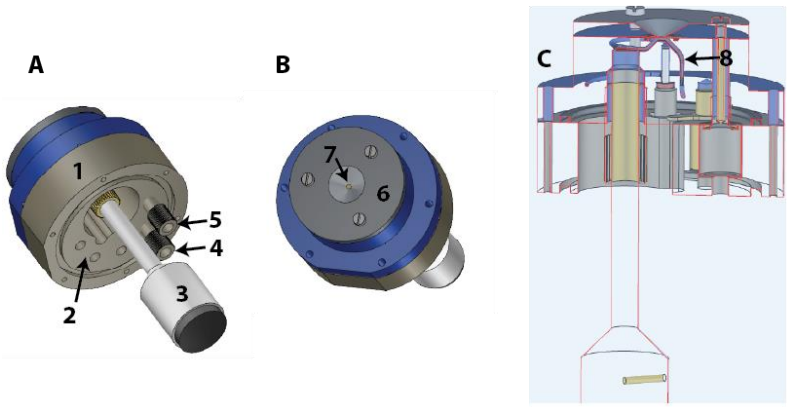

Figure 2.4 : Spectro electrochemical Cell Design for NAP-XPS; A. Side view of the PEEK body of the cell (1), connections for electrolyte (2), the Hydroflex RHE (3), connections for working and Pt counter electrodes (4,5). B. Top view, with the titanium top plate (6) , XPS measurement area (7) and C. Cross-section showing the 3D printed electrolyte channels (8) inside the cell body

PEEK is chosen here because of its high chemical inertness[40]. Meanwhile, 3D printing has the key advantage that connections and electrolyte lines can be shaped in any form with very little restrictions from the manufacturing method. The cell has several other salient features: i) It offers a compact design where all the electrolyte connections, the electrical connections and the reference electrode can be conveniently situated at the backside of the cell outside the vacuum, ii) the cell can be built as one piece with a minimal amount of connections, and iii) the cell has a very small internal volume which facilitates quick switching to a different electrolyte and limits the amount of electrolyte that can spill into the vacuum chamber in event of a leakage

The potentiostat connections for the electrodes as well as the electrolyte supply and return lines are connected to the fixed part of the manipulator. The electrolyte connections (2) are present at the rear of the cell and are connected to the electrolyte supply and return lines that run through the inner tube of the manipulator. As a safety precaution, individual SOVs (Solenoid Operated Valves) are installed on each electrolyte line, immediately cutting off the electrolyte supply upon detecting an electrolyte leak from the cell into the main chamber. These, in addition to other safety interlocks, are discussed in the supplementary information A2.5.

All the surfaces of the electrochemical manipulator that come in contact with the electrolyte can be cleaned to according to regular electrochemical lab standards using acidified $KMnO_4$, dilute piranha solution (H_2SO_4+H_2O_2) and warm water. We note that such cleaning is crucial to ensure well-controlled electrochemistry inside the cell and reliable Spectro-electrochemical results. Detailed cleaning process is explained in the supplementary information A2.7.

ii) Membrane electrode assembly (MEA)

The samples used in the electrochemical cell are a special type of membrane electrode assembly based on the design developed at ISSIS Beamline at BESSY-II [21,41]. In short, the electrocatalyst of choice is deposited on membrane, which can either be porous or a polymer electrolyte (Figure 2.5). Subsequently, the catalyst is covered with a bilayer of graphene. During the electrochemical XPS measurements, the membrane-catalyst-graphene assembly is in contact with electrolyte from the backside of the membrane. This electrolyte can permeate through the membrane in order to reach the catalyst, providing electrochemical contact. Meanwhile, the graphene functions as an evaporation barrier, so that a liquid film is maintained around the catalyst particles. In previous work[41], our assembly was based on polymer ion-exchange membranes (e.g Nafion), which only allow water molecules and protons to pass through to the working electrode. Here, we make use of a porous polycarbonate (PC) membrane (50 nm pore size Polycarbonate PVP treated Membrane, it4ip SA), which allows any molecule or ion to reach the electrocatalyst. This makes it possible to study a much wider array of electrochemical reactions, as will be exemplified below for the oxygen reduction reaction. Importantly, the porous PC membrane is chemically stable against both low and high pH.

Figure 2.6 shows scanning electron microscope images of the MEAs in 'as prepared' state and after an XPS experiment. The as prepared sample (Figure 2.6 A) shows an evenly distributed thin catalyst layer mixed with the 50 nm pores that are visible as black. Images following 6-8 hours of voltametric measurements and XPS measurements (Figure 2.6 B) show essentially the same configuration, but with a more pronounced cracking pattern due to physical strain on the MEA once it is pressed under the top plate of the electrochemical cell and potentially slight catalyst degradation. Note that in both cases, the graphene cannot be discerned due to the high magnification and uniformity of the graphene layer in the region imaged. However, the SEM images collected at lower magnifications and in different regions on the graphene-Pt-membrane assembly clearly shown the presence of the graphene layer (additional images in supplementary information A2.9). Additionally, a strong aromatic C 1s peak from the graphene can be seen in the survey spectrum (Figure 2.11). Corresponding cyclic voltammograms to these SEM images show characteristic Pt peaks in both the cases, although the latter having smaller peak currents which may be attributed to Pt catalyst degradation mechanisms such as dissolution and Ostwald ripening[42–47]. Importantly, these measurements show that prolonged electrochemical contact can be maintained even under circumstances where electrode degradation occurs.

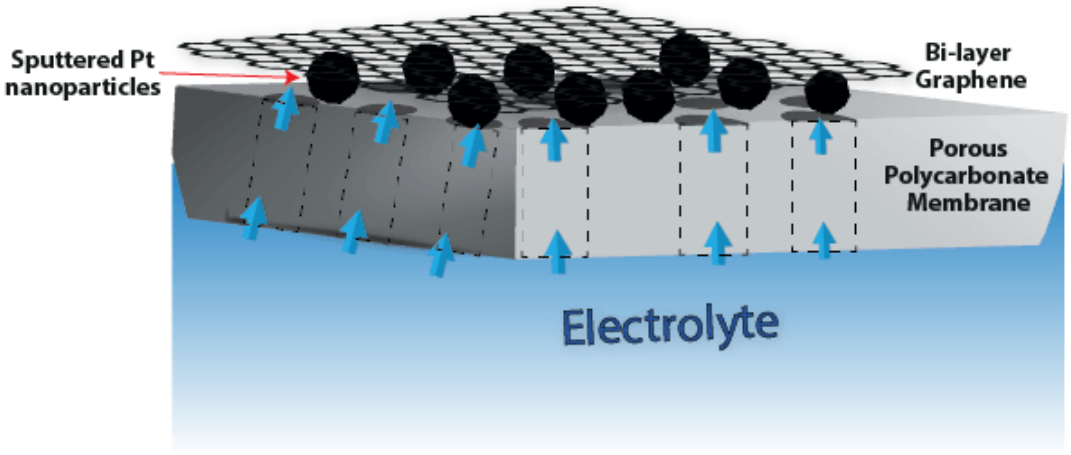

Figure 2.5 : Schematic diagram of Graphene-Platinum-Polycarbonate membrane assembly

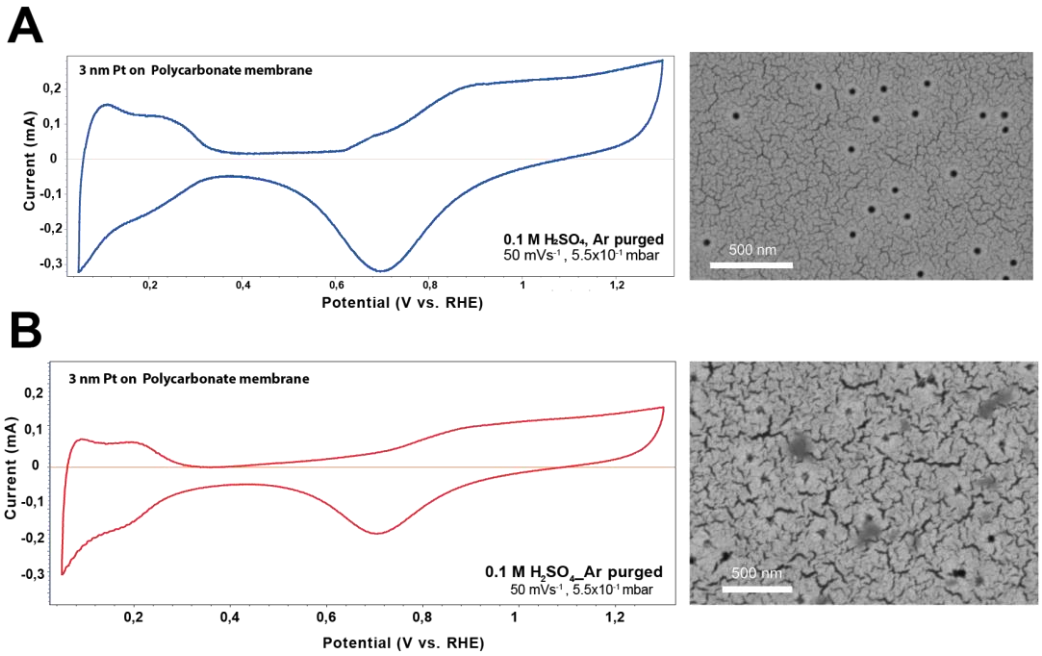

Figure 2.6 : SEM Images recorded for Graphene-Platinum-Membrane Assembly as prepared (A) and following 6-8 hours of spectro-electrochemical measurements in dilute acidic media (B) shown with their corresponding cyclic voltammograms

To test the mass transport through the porous membrane, we conducted oxygen reduction electrocatalysis experiments. Note that this is an extreme test, because the reactant O_2 can only be dissolved in the electrolyte in extremely low concentrations. Nonetheless, Figure 2.7 shows a clear response to the presence/absence of O_2 in the electrolyte, confirming that O_2 is readily transported through the porous membrane to the electrode under in situ XPS conditions. However, it should be noted that the response is small indicating that some mass transport limitations do exist, as can be expected based on sample geometry observed in Figure 2.5. Nonetheless, the oxygen permeation experiment highlights the possibility of studying a wide variety of electrochemical reactions in the NAP-XPS set-up, including those with neutral molecules or dissolved gases.

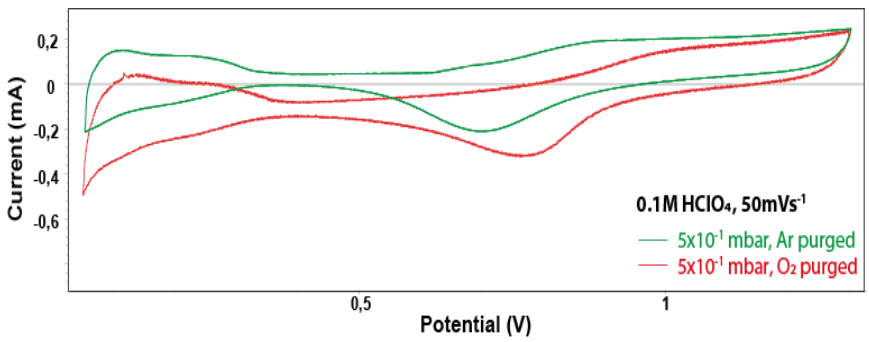

Figure 2.7 : Oxygen permeation behavior of the 50 nm pore size Polycarbonate membrane evidenced by the voltametric response of Pt, showing effect of equilibrium oxygen concentration under ambient and rough vacuum pressures

2.3 Experimental methods

To conduct proof-of-concept measurements, 3 nm Pt was sputtered onto a porous polycarbonate membrane (50 nm pore size Polycarbonate PVP treated Membrane, it4ip SA) using a Cressington sputter coater. In-house prepared graphene was transferred onto membrane-catalyst assembly according to previously established procedure[21] and stored dry. Prior to use in an in situ experiment, the sample is immersed in ultrapure water for ~15 minutes to hydrate the pores. The membrane-catalyst-graphene assembly is mounted on the cell with the graphene is centered on the XPS measurement area, facing the vacuum side (Figure 2.8). The electrochemistry is controlled using a SP-200 Biologic potentiostat. This allows us to perform all the standard electrochemical techniques within the operando spectroscopic experiment, ranging from performing simple cyclic voltammograms, pulse voltammograms, linear sweep voltammograms to more complex experiments involving a series of these techniques one after the other during the XPS operation.

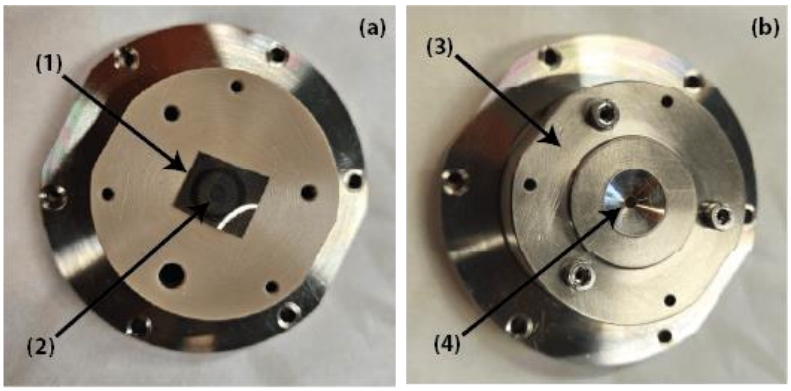

Figure 2.8 : Membrane electrode assembly mounting on the EC cell; (a) Graphene-Platinum-Membrane assembly has to be centered on the electrolyte channel (b) Titanium top plate is mounted as an electrical contact to the membrane

Once electrolyte circulation is established, the sample is placed inside the load lock and pumped to rough vacuum while checking for visible leaks. Proper electrochemistry under vacuum conditions is verified using the (stable) open circuit potential and cyclic voltammetry. After placing the sample in the cell and establishing the electrolyte circulation at a steady state, a cyclic voltammogram was measured between 0.05 V_{RHE} – 1.3 V_{RHE} at 50 mVs^{-1} to remove any memory effects and to know the electrochemically active surface area of the deposited Pt nano-particles. The cell position is optimized with respect to the X-ray source and the analyzer nozzle using a high-resolution camera and the XPS count rate (see Figure 2.9).

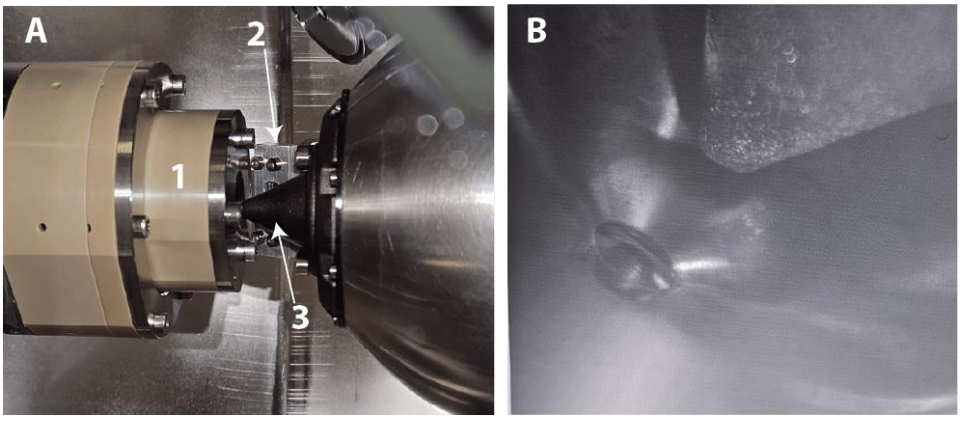

Figure 2.9 : Electrochemical cell alignment; A) shows the EC-XPS cell (1) aligned with the X-ray source NAP extension (2) and the analyzer nozzle (3) and B) shows fine tuning of the sample distance with the analyzer nozzle

2.4 Results

i) Pt Oxidation in Acidic Media

In this section, we demonstrate that the lab-based electrochemical NAP-XPS that we have commissioned is capable of conducting in situ studies on Pt oxidation using a lab-scale X-ray source. The precise nature of Pt oxidation is an important topic in electrocatalysis due to e.g. its implications on fuel cell stability[48,49]. In previous work, we have studied Pt oxidation using synchrotron facilities [21,35,41], allowing for a direct comparison.

As a first step, we benchmarked the electrochemical behavior of the membrane-Pt-graphene assembly by comparison to graphite-supported Pt nanoparticles in a conventional glass cell. Figure 2.10 shows the cyclic voltammograms for the glass cell and the Spectro-electrochemical cell side by side. Clearly, very similar behavior is observed, confirming the proper electrochemical performance of the in situ spectroscopy cell. The small differences that can be observed are likely related to the difference in support effect between the glassy carbon electrode and the polycarbonate membrane.

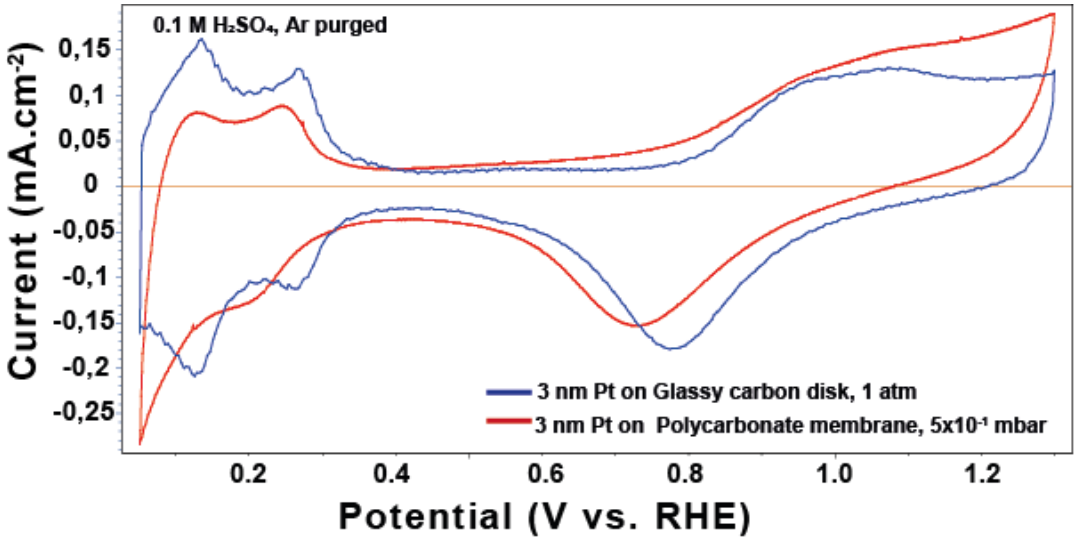

Figure 2.10 : Cyclic Voltammograms on 3 nm Pt nano-particles in glass cell (blue curve) using a glassy carbon support and (red curve) in EC-XPS flow cell using PC membrane support

The low leak rate of the cell and membrane-catalyst-graphene assembly is verified using the chamber pressure: ~1x10^{-1} mbar only being pumped through the 300 µm analyzer nozzle. This leak rate is achieved for both high and low pH electrolyte and any electrode potential. An advantage of the low chamber pressure is that there is minimal signal loss due to photoelectron-gas scattering.

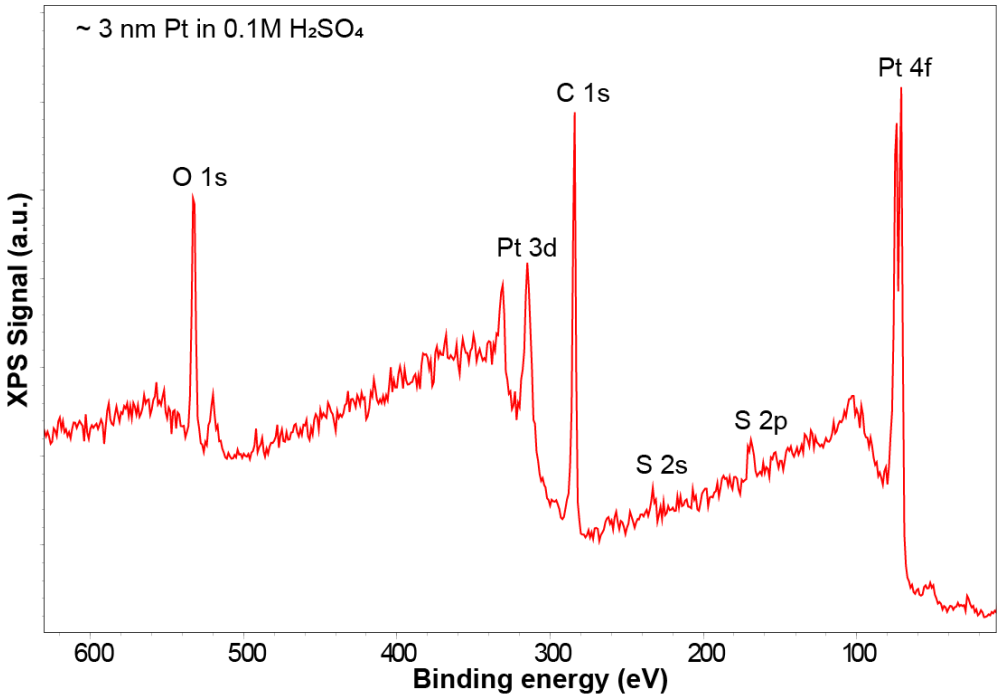

Figure 2.11 : XPS Survey spectrum for the membrane electrode assembly in acidic electrolyte (0.1M H_2SO_4)

A survey spectrum was recorded prior to the anodization (Figure 2.11) which shows the expected elemental contributions from the aqueous electrolyte (O 1s), the catalyst (Pt 4f) and the support (C 1s and O 1s). C 1s appears as one of the most intense peaks, which mainly arises from the bilayer graphene covering the MEA and partially from the polycarbonate membrane support, which also contributes partially to the O 1s signal. XPS spectra are measured by anodizing the sample in steps, while recording spectra at each step potential (Figure 2.12). Pt 4f spectra were recorded at 10 eV analyzer pass energy with an acquisition time of ~5 min. The Pt spectra were fitted using different oxidation states of Pt; Pt^0 (Pt $4f_{7/2}$ at 71.0 eV), $Pt^{\delta+}$(71.8 eV), Pt^{2+}(72−72.7 eV) and Pt^{4+}(73.7 eV) doublets (the details of the curve fitting parameters are given in supplementary information A2.8.

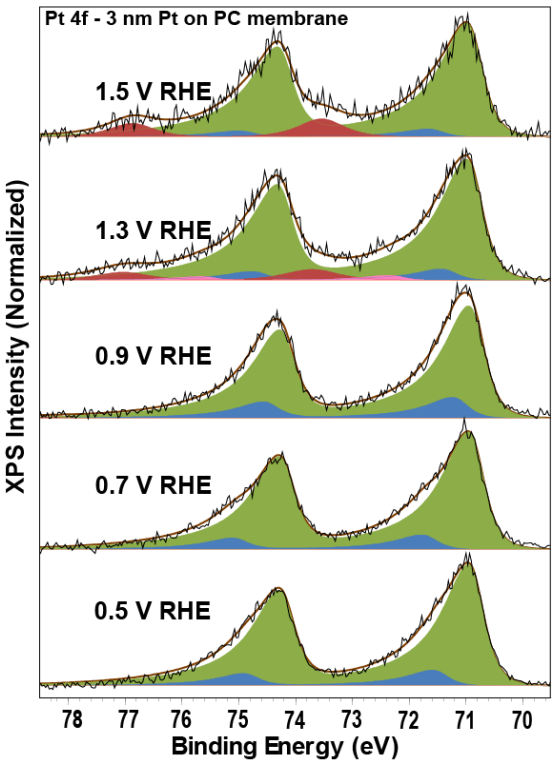

Figure 2.12 : Step-wise anodization of the Pt-nano particles in 0.1 M H_2SO_4, Pt 4f spectra are fit using Pt^0 (green), $Pt^{\delta+}$ (blue), Pt^{2+} (pink), and Pt^{4+} (red) doublets.

At 0.5 V_{RHE}, the XPS spectra in Figure 2.12 show large contributions from metallic Pt and $Pt^{\delta+}$. The $Pt^{\delta+}$ contribution at this low potential where no Pt oxides are expected, is related to the presence of adsorbates on the Pt surface, as also observed in our previous work[35,41]. At 1.3 V_{RHE}, Pt is well within its oxidation regime and accordingly, prominent oxidized Pt contributions can be observed. In line with previous work, a mixture of $Pt^{\delta+}$, Pt^{2+}, and Pt^{4+} oxidation states is observed showing that an irregular surface oxide structure is formed. Upon increasing the potential further to 1.5 V_{RHE}, deeper oxidation of the nano-particles is induced which can be seen from a large contribution from Pt^{4+}. It is important to note that based on modeling of the XPS signals, we previously estimated that the oxide film on the particles is approximately one monolayer thick[41]. This was done by modelling the oxide to metal ratios observed in Figure

2.12 as a function of potential using planar and nanoparticle overlayer models[50,51]. Thus the data presented here provide a clear showcase of the sensitivity that can be reached using lab-based electrochemical XPS.

A key feature of electrochemical XPS is that not only the chemistry of the electrode can be investigated, but also the behavior of the interfacial electrolyte. The binding energy shift with applied potential for the electrolyte species can be utilized to identify their location with respect to the working electrode[20,35]. This binding energy shift originates from the change in the electrostatic potential experienced by the electrolyte when a potential is applied (see Figure 2.13). When the electrode is grounded, the shift for bulk electrolyte species (outside of the double layer) is described as:

$$E_{binding,apparent} = E_{binding,actual} + q_e \Delta U \qquad (1)$$

Where $E_{binding,apparent}$ and $E_{binding,actual}$ show the observed and the real binding energies of the electrolyte species, q_e is the charge of an electron and ΔU is the change in the electrolyte potential with respect to the setup. *Equation 1* indicates that bulk electrolyte species shift -1 eV when the electrode potential is increased by 1 V. In the double layer, the shift progressively reduces the closer the electrolyte species is to the electrode surface.

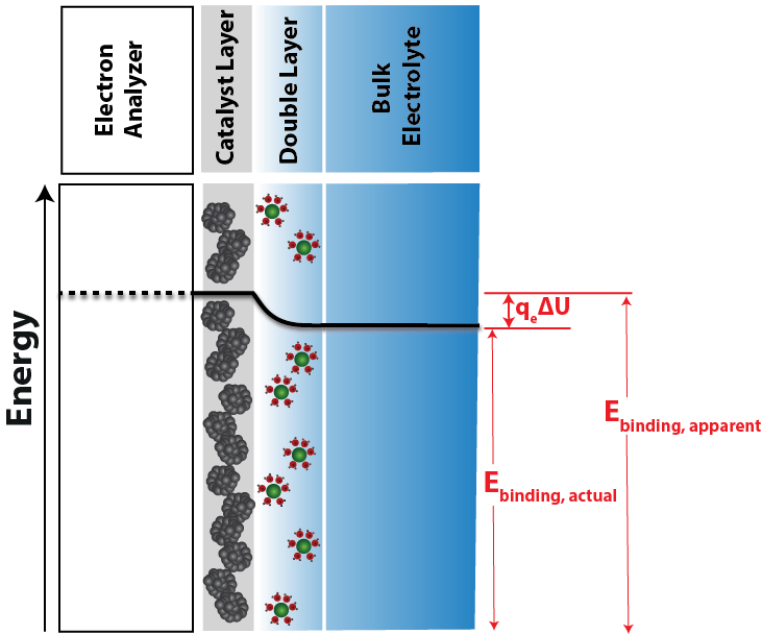

Figure 2.13: Difference between apparent and real binding energies as a result of change in the electrolyte potential. The product of electronic charge 'q_e' and change in electrolyte potential 'ΔU' equals the difference between apparent and real binding energies

The potential-dependent effect is clearly observed in O 1s spectra (Figure 2.14), which are dominated by water. Based on the ~-1 eV/V_{RHE} binding energy shift observed, it is clear that most of the probed water molecules are not located in the double layer. This is consistent with recent measurements on the double layer of the 0.1 M H_2SO_4 – RuO_2 interface, where it was

shown that the double layer is <1 nm[20], well below the probing depth of our XPS in liquid water[52]. The -1:1 shift for H_2O, but the lack of such a shift for the grounded Pt electrode establish that a proper electrode-electrolyte interface is formed in our cell.

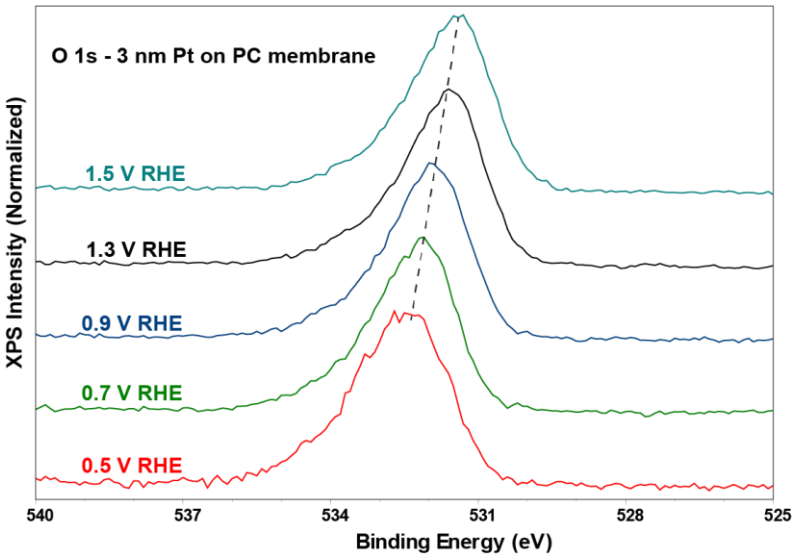

Figure 2.14 : Binding energy shift for O 1s spectra as a function of potential

Since the experiment was done in 0.1 M H_2SO_4, it is also important to track the contribution of sulfur as a function of polarization (Figure 2.15). It can be clearly observed that the sulfate S 2p does not shift in the same way as the water O 1s peak. This can be explained by the fact that sulfate is known to adsorb on Pt electrodes (contributing to the $Pt^{\delta+}$ observed in the Pt 4f spectra). As a consequence, the sulfate ions are grounded to the working electrode and do not experience any electrostatic potential shift with increasing applied potential. As small S 2p shift can be observed for the spectra at 1.3 V_{RHE} and 1.5 V_{RHE} spectra, however. This shift is likely related to the different chemical environment experience by sulfate ions when adsorbed on metallic Pt (<1.3 V_{RHE}) vs. on PtO_x (at or above 1.3 V_{RHE}).

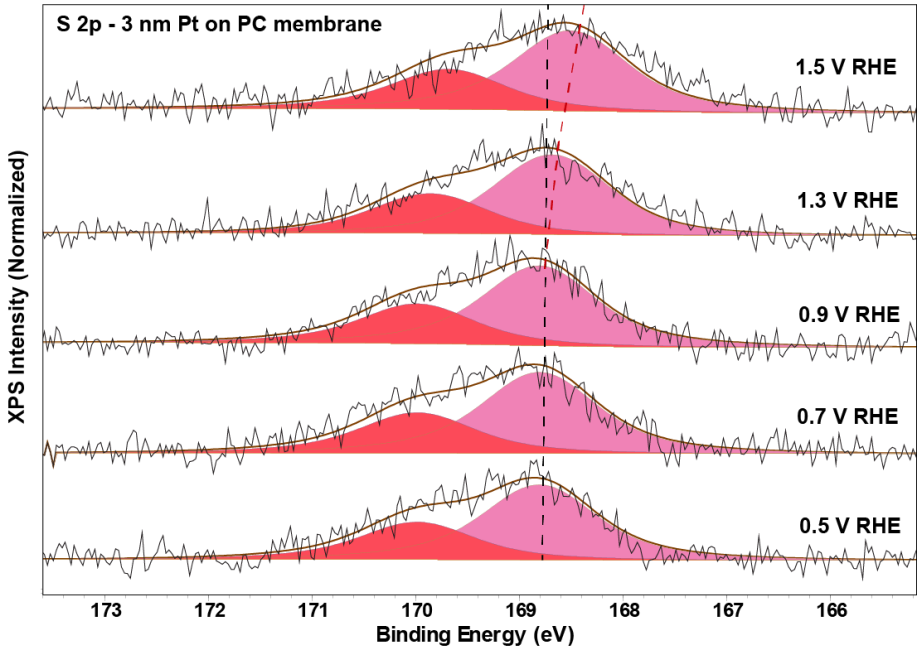

Figure 2.15 : Step-wise anodization of the Pt-nano particles in 0.1 M H_2SO_4, S 2p spectra are fit using pink and red doublets. Black dashed line shows an absence of a spectral shift at lower potentials while deviating red dashed line shows a binding shift at higher potentials due to changing nature of chemical interaction between sulfate and Pt oxides

With the case study on Pt oxidation, we showcase how our laboratory-based electrochemical XPS system is able to resolve both sides of the electrode-electrolyte interface. Exploiting the chemical stability of the polycarbonate support and its non-selective electrolyte conduction to the working electrode, a wide range of chemical reactions could be studied using the setup under *operando* conditions.

2.5 Conclusion

We have described a lab-based electrochemical NAP-XPS instrument optimized for electrocatalysis studies. The instrument is specifically designed to 1) facilitate measurements on a wide variety of electrochemical reactions under *operando* conditions, 2) enable simple, clean and (vacuum) safe operation, and 3) allow for fast sample and electrolyte exchange. Key to the design is the use of a spectro-electrochemical cell based on a membrane-electrode-graphene assembly. We show that this assembly facilitates measurements on all components of the electrode-electrolyte interface for any nanoparticle electrocatalyst and any aqueous electrolyte. Furthermore, we show that the membrane-catalyst-graphene assembly allows adequate mass transport of reactants, even for reactions involving dissolved gasses, as exemplified for the oxygen reduction reaction. We foresee that the step from the synchrotron to the lab is key for integrating electrochemical XPS into the electrochemist's toolbox, enabling a day-to-day feedback loop with the electrochemical lab.

References

(1) Handoko, A. D.; Wei, F.; Jenndy; Yeo, B. S.; Seh, Z. W. Understanding Heterogeneous Electrocatalytic Carbon Dioxide Reduction through Operando Techniques. *Nature Catalysis*. Nature Publishing Group December 1, 2018, pp 922–934. https://doi.org/10.1038/s41929-018-0182-6.

(2) Chu, S.; Cui, Y.; Liu, N. The Path towards Sustainable Energy. *Nature Materials*. Nature Publishing Group December 20, 2016, pp 16–22. https://doi.org/10.1038/nmat4834.

(3) Wakisaka, M.; Asizawa, S.; Watanabe, M.; Uchida, H.; Watanabe, M. In Situ STM Observation of Morphological Changes of the Pt(111) Electrode Surface during Potential Cycling in 10 MM HF Solution. *Physical Chemistry Chemical Physics* **2010**, *12* (16), 4184–4190. https://doi.org/10.1039/b923956a.

(4) Marković, N. M.; Ross, P. N. Surface Science Studies of Model Fuel Cell Electrocatalysts. *Surf Sci Rep* **2002**, *45* (4–6), 117–229. https://doi.org/10.1016/s0167-5729(01)00022-x.

(5) Nguyen, L.; Tao, F. F.; Tang, Y.; Dou, J.; Bao, X. J. Understanding Catalyst Surfaces during Catalysis through Near Ambient Pressure X-Ray Photoelectron Spectroscopy. *Chemical Reviews*. American Chemical Society June 26, 2019, pp 6822–6905. https://doi.org/10.1021/acs.chemrev.8b00114.

(6) Opitz, A. K.; Nenning, A.; Rameshan, C.; Kubicek, M.; Götsch, T.; Blume, R.; Hävecker, M.; Knop-Gericke, A.; Rupprechter, G.; Klötzer, B.; Fleig, J. Surface Chemistry of Perovskite-Type Electrodes during High Temperature CO2 Electrolysis Investigated by Operando Photoelectron Spectroscopy. *ACS Appl Mater Interfaces* **2017**, *9* (41), 35847–35860. https://doi.org/10.1021/acsami.7b10673.

(7) Opitz, A. K.; Nenning, A.; Rameshan, C.; Rameshan, R.; Blume, R.; Hävecker, M.; Knop-Gericke, A.; Rupprechter, G.; Fleig, J.; Klötzer, B. Enhancing Electrochemical Water-Splitting Kinetics by Polarization-Driven Formation of near-Surface Iron(0): An in Situ XPS Study on Perovskite-Type Electrodes. *Angewandte Chemie - International Edition* **2015**, *54* (9), 2628–2632. https://doi.org/10.1002/anie.201409527.

(8) Zhong, L.; Chen, D.; Zafeiratos, S. A Mini Review of in Situ Near-Ambient Pressure XPS Studies on Non-Noble, Late Transition Metal Catalysts. *Catalysis Science and Technology*. Royal Society of Chemistry 2019, pp 3851–3867. https://doi.org/10.1039/c9cy00632j.

(9) Stevie, F. A.; Donley, C. L. Introduction to X-Ray Photoelectron Spectroscopy. *Journal of Vacuum Science & Technology A: Vacuum, Surfaces, and Films* **2020**, *38* (6). https://doi.org/10.1116/6.0000412.

(10) Ketenoglu, D. A General Overview and Comparative Interpretation on Element-Specific X-Ray Spectroscopy Techniques: XPS, XAS, and XRS. *X-Ray Spectrometry* **2022**, *51* (5–6), 422–443. https://doi.org/10.1002/xrs.3299.

(11) Baraldi, A.; Comelli, G.; Lizzit, S.; Kiskinova, M.; Paolucci, G. Real-Time X-Ray Photoelectron Spectroscopy of Surface Reactions. *Surface Science Reports*. Elsevier 2003, pp 169–224. https://doi.org/10.1016/S0167-5729(03)00013-X.

(12) Babenkov, S. V.; Aristov, V. Y.; Molodtsova, O. V.; Winkler, K.; Glaser, L.; Shevchuk, I.; Scholz, F.; Seltmann, J.; Viefhaus, J. A New Dynamic-XPS End-Station for Beamline P04 at PETRA III/DESY. *Nucl Instrum Methods Phys Res A* **2015**, *777*, 189–193. https://doi.org/10.1016/j.nima.2014.12.065.

(13) Salmeron, M. From Surfaces to Interfaces: Ambient Pressure XPS and Beyond. *Top Catal* **2018**, *61* (20), 2044–2051. https://doi.org/10.1007/s11244-018-1069-0.

(14) Arrigo, R.; Hävecker, M.; Schuster, M. E.; Ranjan, C.; Stotz, E.; Knop-Gericke, A.; Schlögl, R. In Situ Study of the Gas-Phase Electrolysis of Water on Platinum by NAP-XPS. *Angewandte Chemie - International Edition* **2013**, *52* (44), 11660–11664. https://doi.org/10.1002/anie.201304765.

(15) Favaro, M.; Jeong, B.; Ross, P. N.; Yano, J.; Hussain, Z.; Liu, Z.; Crumlin, E. J. Unravelling the Electrochemical Double Layer by Direct Probing of the Solid/Liquid Interface. *Nat Commun* **2016**, *7*. https://doi.org/10.1038/ncomms12695.

(16) Temperton, R. H.; Kawde, A.; Eriksson, A.; Wang, W.; Kokkonen, E.; Jones, R.; Gericke, S. M.; Zhu, S.; Quevedo, W.; Seidel, R.; Schnadt, J.; Shavorskiy, A.; Persson, P.; Uhlig, J. Dip-and-Pull Ambient Pressure Photoelectron Spectroscopy as a Spectroelectrochemistry Tool for Probing Molecular Redox Processes. *Journal of Chemical Physics* **2022**, *157* (24). https://doi.org/10.1063/5.0130222.

(17) Teschner, D.; Plescher, J.; Piccinin, S.; Jones, T. E.; Hammud, A.; Schmidt, F.; Knop-Gericke, A.; Bluhm, H.; Shavorskiy, A. Understanding Anomalous Gas-Phase Peak Shifts in Dip-and-Pull Ambient Pressure XPS Experiments. *Journal of Physical Chemistry C* **2024**. https://doi.org/10.1021/acs.jpcc.4c00113.

(18) Capone, F. G.; Sottmann, J.; Meunier, V.; Pérez Ramírez, L.; Grimaud, A.; Iadecola, A.; Scardamaglia, M.; Rueff, J. P.; Dedryvère, R. Operando Observation of the Dynamic SEI Formation on a Carbonaceous Electrode by Near-Ambient Pressure XPS. *Energy Environ Sci* **2024**, *17* (4), 1509–1519. https://doi.org/10.1039/d3ee03228k.

(19) Casalongue, H. S.; Kaya, S.; Viswanathan, V.; Miller, D. J.; Friebel, D.; Hansen, H. A.; Nørskov, J. K.; Nilsson, A.; Ogasawara, H. Direct Observation of the Oxygenated Species during Oxygen Reduction on a Platinum Fuel Cell Cathode. *Nat Commun* **2013**, *4*. https://doi.org/10.1038/ncomms3817.

(20) Velasco-Velez, J. J.; Falling, L. J.; Bernsmeier, D.; Sear, M. J.; Clark, P. C. J.; Chan, T. S.; Stotz, E.; Hävecker, M.; Kraehnert, R.; Knop-Gericke, A.; Chuang, C. H.; Starr, D. E.; Favaro, M.; Mom, R. V. A Comparative Study of Electrochemical Cells for in Situ X-Ray Spectroscopies in the Soft and Tender x-Ray Range. *J Phys D Appl Phys* **2021**, *54* (12). https://doi.org/10.1088/1361-6463/abd2ed.

(21) Falling, L. J.; Mom, R. V.; Sandoval Diaz, L. E.; Nakhaie, S.; Stotz, E.; Ivanov, D.; Hävecker, M.; Lunkenbein, T.; Knop-Gericke, A.; Schlögl, R.; Velasco-Vélez, J. J. Graphene-Capped Liquid Thin Films for Electrochemical Operando X-Ray Spectroscopy and Scanning Electron Microscopy. *ACS Appl Mater Interfaces* **2020**, *12* (33), 37680–37692. https://doi.org/10.1021/acsami.0c08379.

(22) Weatherup, R. S.; Eren, B.; Hao, Y.; Bluhm, H.; Salmeron, M. B. Graphene Membranes for Atmospheric Pressure Photoelectron Spectroscopy. *Journal of Physical Chemistry Letters* **2016**, *7* (9), 1622–1627. https://doi.org/10.1021/acs.jpclett.6b00640.

(23) Kolmakov, A.; Dikin, D. A.; Cote, L. J.; Huang, J.; Abyaneh, M. K.; Amati, M.; Gregoratti, L.; Günther, S.; Kiskinova, M. Graphene Oxide Windows for in Situ Environmental Cell Photoelectron Spectroscopy. *Nat Nanotechnol* **2011**, *6* (10), 651–657. https://doi.org/10.1038/nnano.2011.130.

(24) Stoerzinger, K. A.; Favaro, M.; Ross, P. N.; Hussain, Z.; Liu, Z.; Yano, J.; Crumlin, E. J. Stabilizing the Meniscus for Operando Characterization of Platinum During the Electrolyte-Consuming Alkaline Oxygen Evolution Reaction. *Top Catal* **2018**, *61* (20), 2152–2160. https://doi.org/10.1007/s11244-018-1063-6.

(25) Ali-Löytty, H.; Louie, M. W.; Singh, M. R.; Li, L.; Sanchez Casalongue, H. G.; Ogasawara, H.; Crumlin, E. J.; Liu, Z.; Bell, A. T.; Nilsson, A.; Friebel, D. Ambient-Pressure XPS Study of a Ni-Fe Electrocatalyst for the Oxygen Evolution Reaction. *Journal of Physical Chemistry C* **2016**, *120* (4), 2247–2253. https://doi.org/10.1021/acs.jpcc.5b10931.

(26) Favaro, M.; Drisdell, W. S.; Marcus, M. A.; Gregoire, J. M.; Crumlin, E. J.; Haber, J. A.; Yano, J. An Operando Investigation of (Ni-Fe-Co-Ce)Ox System as Highly Efficient Electrocatalyst for Oxygen Evolution Reaction. *ACS Catal* **2017**, *7* (2), 1248–1258. https://doi.org/10.1021/acscatal.6b03126.

(27) Wang, Y.; Wang, W.; Xie, J.; Wang, C. H.; Yang, Y. W.; Lu, Y. C. Electrochemical Reduction of CO2 in Ionic Liquid: Mechanistic Study of Li–CO2 Batteries via in Situ Ambient Pressure X-Ray Photoelectron Spectroscopy. *Nano Energy* **2021**, *83*. https://doi.org/10.1016/j.nanoen.2021.105830.

(28) Permyakova, A. A.; Herranz, J.; El Kazzi, M.; Diercks, J. S.; Povia, M.; Mangani, L. R.; Horisberger, M.; Pătru, A.; Schmidt, T. J. On the Oxidation State of Cu2O upon Electrochemical CO2 Reduction: An XPS Study. *ChemPhysChem* **2019**, *20* (22), 3120–3127. https://doi.org/10.1002/cphc.201900468.

(29) Liu, C.; Dong, Q.; Han, Y.; Zang, Y.; Zhang, H.; Xie, X.; Yu, Y.; Liu, Z. Understanding Fundamentals of Electrochemical Reactions with Tender X-Rays: A New Lab-Based Operando X-Ray Photoelectron Spectroscopy Method for Probing Liquid/Solid and Gas/Solid Interfaces across a Variety of Electrochemical Systems. *Chinese Journal of Catalysis* **2022**, *43* (11), 2858–2870. https://doi.org/10.1016/S1872-2067(22)64092-0.

(30) Griesser, C.; Winkler, D.; Moser, T.; Haug, L.; Thaler, M.; Portenkirchner, E.; Klötzer, B.; Diaz-Coello, S.; Pastor, E.; KunzeLiebhäuser, J. Lab-Based Electrochemical X-Ray Photoelectron Spectroscopy for in-Situ Probing of Redox Processes at the Electrified Solid/Liquid Interface. *Electrochemical Science Advances* **2023**. https://doi.org/10.1002/elsa.202300007.

(31) Jürgensen, A.; Esser, N.; Hergenröder, R. Near Ambient Pressure XPS with a Conventional X-Ray Source. In *Surface and Interface Analysis*; 2012; Vol. 44, pp 1100–1103. https://doi.org/10.1002/sia.4826.

(32) Arble, C.; Jia, M.; Newberg, J. T. Lab-Based Ambient Pressure X-Ray Photoelectron Spectroscopy from Past to Present. *Surface Science Reports*. Elsevier B.V. May 1, 2018, pp 37–57. https://doi.org/10.1016/j.surfrep.2018.02.002.

(33) Haug, L.; Griesser, C.; Thurner, C. W.; Winkler, D.; Moser, T.; Thaler, M.; Bartl, P.; Rainer, M.; Portenkirchner, E.; Schumacher, D.; Dierschke, K.; Köpfle, N.; Penner, S.; Beyer, M. K.; Loerting, T.; Kunze-Liebhäuser, J.; Klötzer, B. A Laboratory-Based Multifunctional near Ambient Pressure X-Ray Photoelectron Spectroscopy System for Electrochemical, Catalytic, and Cryogenic Studies. *Review of Scientific Instruments* **2023**, *94* (6). https://doi.org/10.1063/5.0151755.

(34) Plodinec, M.; Knop-gericke, A.; Schlo, R.; Jones, T. E. In Situ X - Ray Spectroscopy of the Electrochemical Development Of. *Journal of Physical Chemistry C* **2019**, *123* (1), 9146–9152. https://doi.org/10.1021/acs.jpcc.9b00731.

(35) Mom, R.; Frevel, L.; Velasco-Vélez, J. J.; Plodinec, M.; Knop-Gericke, A.; Schlögl, R. The Oxidation of Platinum under Wet Conditions Observed by Electrochemical X-Ray Photoelectron Spectroscopy. *J Am Chem Soc* **2019**, *141* (16), 6537–6544. https://doi.org/10.1021/jacs.8b12284.

(36) Frevel, L. J.; Mom, R.; Velasco-Vélez, J. J.; Plodinec, M.; Knop-Gericke, A.; Schlögl, R.; Jones, T. E. In Situ X-Ray Spectroscopy of the Electrochemical Development of Iridium Nanoparticles in Confined Electrolyte. *Journal of Physical Chemistry C* **2019**, *123* (14), 9146–9152. https://doi.org/10.1021/acs.jpcc.9b00731.

(37) Mom, R. V.; Falling, L. J.; Kasian, O.; Algara-Siller, G.; Teschner, D.; Crabtree, R. H.; Knop-Gericke, A.; Mayrhofer, K. J. J.; Velasco-Vélez, J. J.; Jones, T. E. Operando Structure-Activity-Stability Relationship of Iridium Oxides during the Oxygen Evolution Reaction. *ACS Catal* **2022**, *12* (9), 5174–5184. https://doi.org/10.1021/acscatal.1c05951.

(38) Velasco-Vélez, J. J.; Jones, T. E.; Streibel, V.; Hävecker, M.; Chuang, C. H.; Frevel, L.; Plodinec, M.; Centeno, A.; Zurutuza, A.; Wang, R.; Arrigo, R.; Mom, R.; Hofmann, S.; Schlögl, R.; Knop-Gericke, A. Electrochemically Active Ir NPs on Graphene for OER in Acidic Aqueous Electrolyte Investigated by in Situ and Ex Situ Spectroscopies. *Surf Sci* **2019**, *681* (September 2018), 1–8. https://doi.org/10.1016/j.susc.2018.10.021.

(39) Velasco-Velez, J. J.; Pfeifer, V.; Hävecker, M.; Weatherup, R. S.; Arrigo, R.; Chuang, C.; Stotz, E.; Weinberg, G.; Salmeron, M.; Schlögl, R.; Knop-Gericke, A. Photoelectron Spectroscopy at the Graphene–Liquid Interface Reveals the Electronic Structure of an Electrodeposited Cobalt/Graphene Electrocatalyst. *Angewandte Chemie* **2015**, *127* (48), 14762–14766. https://doi.org/10.1002/ange.201506044.

(40) VICI AG International. *Chemical Resistance PEEK ® and Other Polymers General Reference*. https://www.daichem.co.jp/system/wp-content/themes/daichem2017/pdf/Chemical_resistance_jour.pdf. (accessed 2nd September, 2024)

(41) Javed, H.; Knop-Gericke, A.; Mom, R. V. Structural Model for Transient Pt Oxidation during Fuel Cell Start-up Using Electrochemical X-Ray Photoelectron Spectroscopy. *ACS Appl Mater Interfaces* **2022**, *14* (31), 36238–36245. https://doi.org/10.1021/acsami.2c09249.

(42) Myers, D. J.; Wang, X.; Smith, M. C.; More, K. L.; Soc, J. E.; Myers, D. J.; Wang, X.; Smith, M. C.; More, K. L. Potentiostatic and Potential Cycling Dissolution of Polycrystalline Platinum and Platinum Nano-Particle Fuel Cell Catalysts. *J Electrochem Soc* **2018**, *165* (6), F3178–F3190. https://doi.org/10.1149/2.0211806jes.

(43) Lopes, P. P.; Tripkovic, D.; Martins, P. F. B. D. B. D.; Strmcnik, D.; Ticianelli, E. A.; Stamenkovic, V. R.; Markovic, N. M. Dynamics of Electrochemical Pt Dissolution at Atomic and Molecular Levels. *Journal of Electroanalytical Chemistry* **2017**, *819* (September), 0–1. https://doi.org/10.1016/j.jelechem.2017.09.047.

(44) Holby, E. F.; Morgan, D. Application of Pt Nanoparticle Dissolution and Oxidation Modeling to Understanding Degradation in PEM Fuel Cells. *J Electrochem Soc* **2012**, *159* (5), B578–B591. https://doi.org/10.1149/2.011204jes.

(45) Yu, Y.; Tu, Z.; Zhang, H.; Zhan, Z.; Pan, M. Comparison of Degradation Behaviors for Open-Ended and Closed Proton Exchange Membrane Fuel Cells during Startup and Shutdown Cycles. *J Power Sources* **2011**, *196* (1), 5077–5083. https://doi.org/10.1016/j.jpowsour.2011.01.075.

(46) Zhang, S.; Yuan, X.; Ng, J.; Hin, C.; Wang, H.; Friedrich, K. A.; Schulze, M. A Review of Platinum-Based Catalyst Layer Degradation in Proton Exchange Membrane Fuel Cells. *J Power Sources* **2009**, *194* (1), 588–600. https://doi.org/10.1016/j.jpowsour.2009.06.073.

(47) Yeon, Y.; Cho, E.; Hyeun, J.; Lim, T.; Oh, I.; Kim, S.; Kim, H.; Hyun, J. Degradation of Polymer Electrolyte Membrane Fuel Cells Repetitively Exposed to Reverse Current Condition under Different Temperature. *J Power Sources* **2011**, *196* (23), 9906–9915. https://doi.org/10.1016/j.jpowsour.2011.08.035.

(48) Randrianarizafy, B.; Schott, P.; Gerard, M.; Bultel, Y. Modelling Carbon Corrosion during a PEMFC Startup : Simulation of Mitigation Strategies. **2020**, 10–16. https://doi.org/10.3390/en13092338.

(49) Yu, Y.; Li, H.; Wang, H.; Yuan, X.; Wang, G.; Pan, M. A Review on Performance Degradation of Proton Exchange Membrane Fuel Cells during Startup and Shutdown Processes : Causes , Consequences , and Mitigation Strategies. *J Power Sources* **2012**, *205* (1), 10–23. https://doi.org/10.1016/j.jpowsour.2012.01.059.

(50) Shard, A. G. A Straightforward Method for Interpreting XPS Data from Core-Shell Nanoparticles. *Journal of Physical Chemistry C* **2012**, *116* (31), 16806–16813. https://doi.org/10.1021/jp305267d.

(51) Ertl, G., Küppers, J., & Grasserbauer, M. Low Energy Electrons and Surface Chemistry. *Anal Chim Acta* **1987**, *199* (1), 272–273. https://doi.org/https://doi.org/10.1016/s0003-2670(00)82831-7.

(52) Shinotsuka, H.; Da, B.; Tanuma, S.; Yoshikawa, H.; Powell, C. J.; Penn, D. R. Calculations of Electron Inelastic Mean Free Paths. XI. Data for Liquid Water for Energies from 50 EV to 30 KeV. *Surface and Interface Analysis* **2017**, *49* (4), 238–252. https://doi.org/10.1002/sia.6123.